Nanoscale

Accepted Manuscript

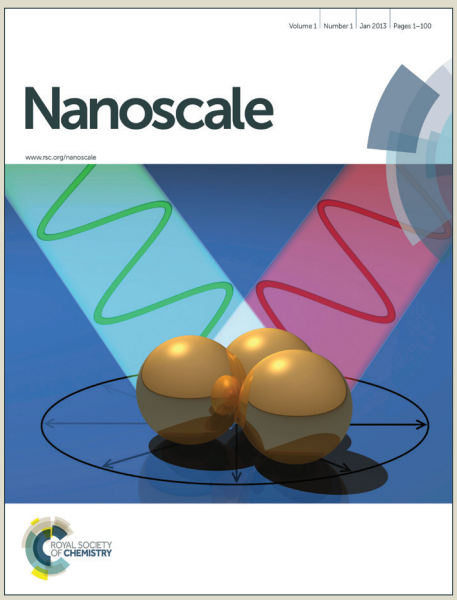

ROYAL SOCIETY OF CHEMISTRY

www.rsc.org/nanoscale

Cite this: DOI: 10.1039/c0xx00000x

www.rsc.org/xxxxxx

ARTICLE TYPE

$NiCo_2S_4$ Sub-Micron Spheres: An Efficient Non-precious Metal Bifunctional Electrocatalyst

Zhongyi Zhang,[a, b, θ] Xiaogang Wang,[a, θ] Guanglei Cui,[a, *] Aihua Zhang,[d] Xinhong Zhou,[c] Hongxia Xu,[a] Lin Gu,[d, *]

Received (in XXX, XXX) Xth XXXXXXXXX 20XX, Accepted Xth XXXXXXXXX 20XX

DOI: 10.1039/b000000x

Urchin-like $NiCo_2S_4$ sub-micron spheres integrated with nano-sized and micro-sized structures, which were synthesized via a facile one-pot method, delivers efficient electrocatalytic activities for oxygen reduction and evolution reaction. The excellent electrocatalytic property of $NiCo_2S_4$ sub-micron spheres is originated from their unique urchin-like microstructure, composition and d-electronic configurations of the transition metal ions.

In the past decades, bifunctional electrocatalysts for oxygen reduction reaction (ORR) and oxygen evolution reaction (OER) are undoubtedly the pivot of advanced energy conversion and storage devices including rechargeable metal-air batteries and regenerative fuel cells.[1-7] Presently, platinum-based electrocatalysts are known to be the preferred electrocatalysts with the highest electrocatalytic activity for ORR.[8] Nevertheless, platinum-based electrocatalysts are generally claimed to be responsible for at least 50% of the total fuel cell cost due to the scarcity and preciousness of platinum.[9] In addition to the high cost of Pt-based electrocatalysts, the limited electrocatalytic activity for OER inhibit their practical application in rechargeable metal-air batteries and regenerative fuel cells.[10-12] Up to now, iridium oxide (IrO_2) and ruthenium oxide (RuO_2) are the best known OER electrocatalysts, unfortunately, which possess poor ORR performance and consist of rarest metal elements.[13-15] Therefore, it is still a big challenge to develop low-cost bifunctional electrocatalysts which can efficiently catalyze both ORR and OER.[4] However, only few articles have been published, covering the synthesis and characteristics of non-precious metal bifunctional electrocatalysts including perovskite and spinel oxides.[3,4,16]

Among various non-precious metal electrocatalysts, late transition metal chalcogenides consisting of transition metal atoms (Fe, Co, Ni) and chalcogen atoms (S, Se, Te) have attracted extensive attentions, because of their low cost, high electrocatalytic activity for ORR and high tolerance to small organic molecules.[17-20] Especially in these chalcogenides, bimetallic sulfides are considered as the most promising catalysts due to the synergistic effect of various transition metal atoms, often exhibiting superior catalytic activity towards many chemical transformations as compared to monometallic sulfides.[21,22] Thiospinels with a general formula of AB_2S_4 is one typical group of bimetallic sulfides, which is known to be built around a closely packed array of S^{2-} ions, with A^{2+} and B^{3+} metal cations occupying the tetrahedral and octahedral sites, respectively.[23-25] Recently, Jin etc. demonstrated that the bifunctional electrocatalytic activities of metal oxides primarily correlate to the σ^*-orbital (e_g) occupation associated with the metal cations at octahedral centers.[3,4] In some cobalt oxides, the surface Co (III) cations are considered to be electrocatalytic active centers for ORR / OER.[4,26] As one of the rare bimetallic thiospinel, $NiCo_2S_4$ with a normal spinel structure is endowed more octahedral catalytic active sites of Co (III) cations compared to $NiCo_2O_4$ with the inverse spinel crystal structure. From this, $NiCo_2S_4$ is potentially provided with excellent bifunctional electrocatalytic activity for both ORR and OER. It is well known that the physicochemical properties of spinels are highly sensitive to the component, structural parameters, and distribution and oxidation state of cations, [16, 27] which depend mostly on the preparation conditions. So far, there are still lacks of viable and facile routes to synthesize $NiCo_2S_4$ with specific nanostructured morphology. Thereby, it is highly challenged and desirable to design and synthesize $NiCo_2S_4$ material as efficient bifunctional electrocatalyst for both ORR and OER.

In this research, urchin-like $NiCo_2S_4$ sub-micron spheres (SMS) were synthesized through a facile one-pot solution-based approach (detailed experiment see supplementary information). These unique urchin-like $NiCo_2S_4$ SMS as non-precious metal electrocatalyst exhibit comparable electrocatalytic activity for ORR and higher electrocatalytic activity for OER compared with commercial Pt/C electrocatalyst in alkaline solutions.

Fig. 1 shows the typical powder X-ray diffraction (XRD) pattern of the as-synthesized $NiCo_2S_4$ SMS. The experimental pattern agrees very well with the standard data of linnaeite-type $NiCo_2S_4$ with a space group of Fd-3m (227) and cubic lattice parameter of a= 9.387 Å (JCPDS card NO. 20-0782).The inset of Fig.1 schematically illustrate the crystal cell structure of $NiCo_2S_4$.

The morphology of the $NiCo_2S_4$ SMS was examined by SEM and TEM. Fig. 2 gives a panoramic picture of the $NiCo_2S_4$ SMS characterized by low-magnification SEM, which shows that the as-synthesized $NiCo_2S_4$ sample consists of almost entirely monodisperse spherical sub-micron particles (100% morphological yield). As shown in Fig. 3a, the $NiCo_2S_4$ sample exhibit uniform morphologies of SMS with an average diameter of 0.25 μm and they present an urchin-like appearance as a whole.

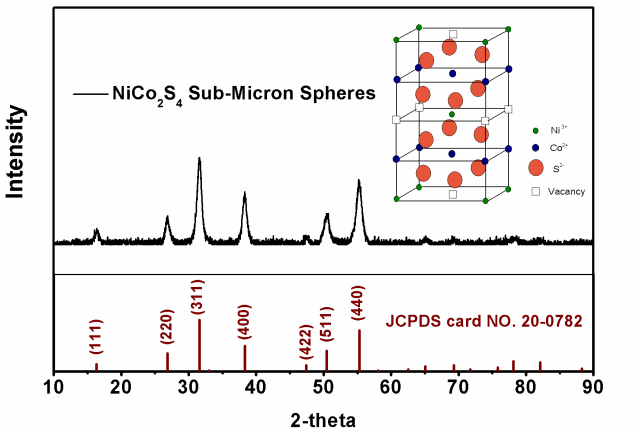

Figure 1 XRD patterns of the as-prepared $NiCo_2S_4$ SMS.

From the TEM image shown in Fig. 3b, it was observed that the surface of the urchin-like $NiCo_2S_4$ SMS is decorated by many nano-papillae primary particles with diameters in the range between 10 to 25 nm in a radial form, expanding the specific surface area of $NiCo_2S_4$ SMS (Fig. S1). Such uniform urchin-like structures not only guarantees desirable mechanical stability of $NiCo_2S_4$ particles but also facilitates the redox species rapidly transport to the electrocatalytic active sites of NiCo2S4 particles. Also, the selected-area electron diffraction (SAED) pattern for a single sphere (Fig. 3c) shows the ring patterns, which are well indexed to planes of (111), (220), (311), (400), (422), (511) and (440). A typical HRTEM image of the nano-papillae primary particles with the corresponding SAED is shown in Fig. 3d. The well-defined crystalline lattice spacing of 2.83 Å is clearly observed, which is consistent with the diffraction peak of (311) plane in the XRD. The elemental mapping images (Fig. 3e~i) did not show any elemental segregation of Ni, Co or S. Energy dispersive spectra (EDS) was used to examine the element composition of the as-prepared $NiCo_2S_4$ SMS (Fig. 3j). It is shown that the atomic ratio of Ni to Co and S is 1.16: 2.00: 3.96, which is approximately the integer ratio of 1: 2: 4, confirming the formation of a stoichiometric $NiCo_2S_4$ compound. The above characterizations of structure and composition credibly demonstrate the as-prepared $NiCo_2S_4$ SMS possess high purity and uniform morphology.

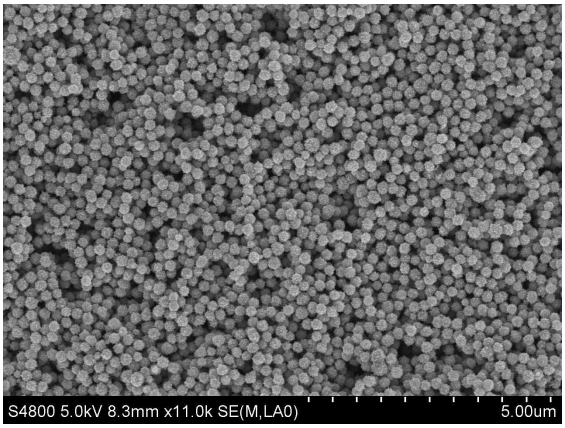

Figure 2 SEM image of the $NiCo_2S_4$ SMS in wide range

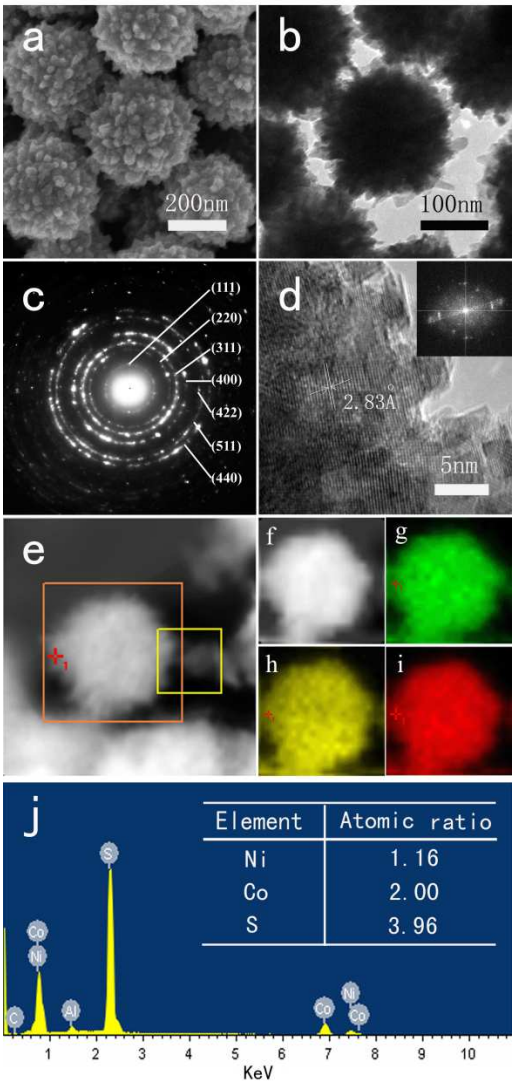

Figure 3 (a) SEM images of the $NiCo_2S_4$ SMS. (b) TEM images of the $NiCo_2S_4$ spheres. (c) SAED patterns for a single $NiCo_2S_4$ sphere. (d) HRTEM images of typical nano-papillae on the surface of the $NiCo_2S_4$ sphere. Inset is the corresponding SAED pattern. (e) Typical STEM image of the $NiCo_2S_4$ SMS. (f) STEM image taken from the square region marked in (e). (g-i) the corresponding elemental mapping images are for

(g) Ni, (h) Co and (i) S, respectively. (j) EDS of the $NiCo_2S_4$ spheres measured by loading on the Al foil.

To understand the formation mechanism of $NiCo_2S_4$ SMS, time-dependent composition and morphology evolution through interception of intermediate products were performed. The SEM images (Fig. 4a~c) show the observed morphologies of intermediate products at three reaction stages. The corresponding reaction stages were marked with I, II and III in Fig. 4d, which exhibits the evolution of various element concentrations with reaction time (based on EDS analysis of intermediate products). As shown in Fig. 4a, the morphology of intermediate products corresponding to reaction stage I can be described as the grass-like configuration. After that, namely in stage II, the grass-like structure dissociated and assembled to form flower-like spheres as shown in Fig. 4b. After 50 minutes reaction that is in stage III, as shown in Fig. 4c, the intermediate products with flower-like

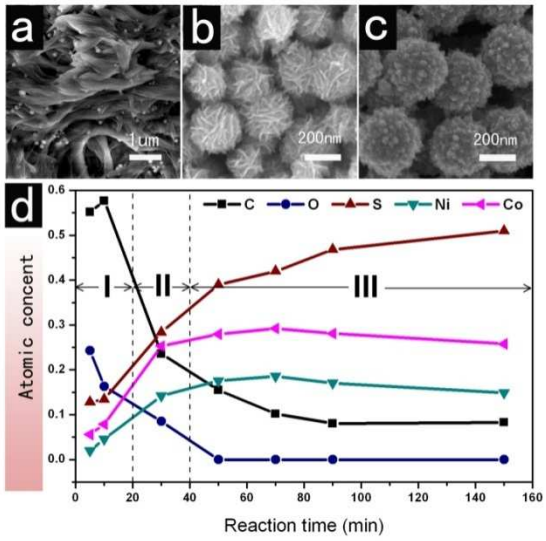

Figure 4 SEM images showing three growth stages of the $NiCo_2S_4$ SMS: (a) Early stage I (b) Middle stage II (c) Final stage III. (d) The plots of element concentrations versus reaction time (based on EDS analysis).

spheres evolved into the final urchin- like SMS. As shown in Fig. 4d, the element concentration of C and O was relatively high in the early stage (I, II) and gradually declined with the reaction progress. This indicates that the reaction is probably accompanied with a decomposition process. After 80 minutes reaction, the element concentration of C and O in the intermediate products gradually decreased to the minimum values. The element concentration of S continuously increased with the slightly decreased element concentrations of Ni and Co. After 120 minutes reaction, the composition and morphology evolution process is accomplished. Consequently, these three elements concentrations attained the stoichiometric value of Ni: Co: S = 1: 2: 4. The sum of element concentrations of Ni, Co and S tended to be more than 90%, which corresponded to above 96% of the total mass content. After 120 minutes, the reaction achieved a high-yield of above 97% for generating $NiCo_2S_4$ SMS (measured by weighting the final products). Thus, the optimum synthesis process was performed at 220 ^oC for 120 minutes.

The electrocatalytic activity of $NiCo_2S_4$ SMS for ORR was characterized by cyclic voltammetry (CV) in 0.1 M KOH aqueous solution on a glassy carbon disk electrode (GC). All electrocatalysts loadings on electrode for electrochemical experiment were uniformly 0.7 mg cm^{-2}. It can be seen from Fig. 5a, the CV curves of $NiCo_2S_4$ SMS obtained in O_2-saturated solution show that the detected currents increased rapidly in the mixed kinetic-diffusion control region (-0.1 V to -0.22 V), then reached the peak value and next gradually decreased. This observed current was attributed to ORR electrocatalyzed by $NiCo_2S_4$ SMS through comparison with CV curve recorded in Ar-saturated aqueous solution, which show no distinguishable cathodic current over the measured potential range. And the CV curves of $NiCo_2S_4$ SMS show that an ORR onset potential at -0.05 V (versus Ag / AgCl electrode) and the peak potential is at -0.22 V. The CV curves of commercial Pt/C electrocatalysts (10 wt.% Pt), as shown in Fig. 5b, exhibit the ORR onset potential and peak potential located at 0.05 V and -0.13 V, respectively.

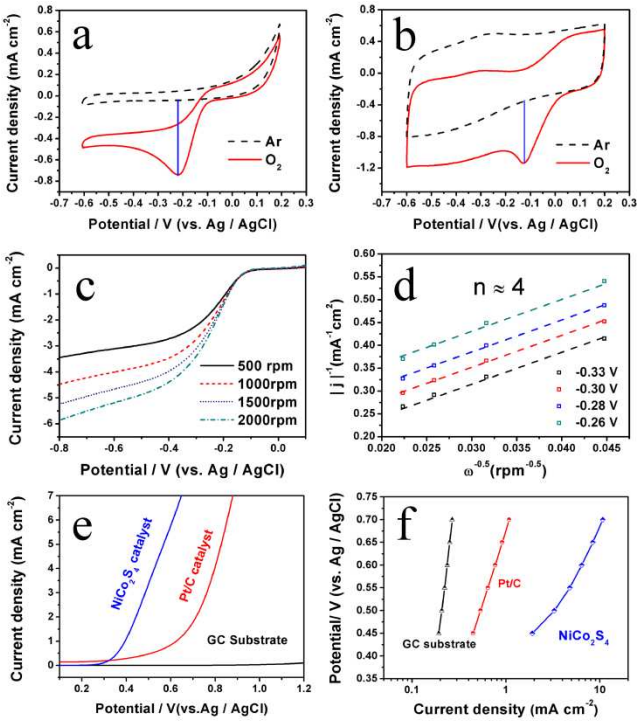

Figure 5 Cyclic voltammetry curves of (a) the $NiCo_2S_4$ and (b) the Pt/C electrocatalyst in Ar or O_2 saturated 0.1 M KOH aqueous solution at a scan rate of 10 mVs^{-1}. (c) LSV curves of the $NiCo_2S_4$ electrocatalyst in O_2-saturated 0.1M KOH aqueous solution at different rotation rate with a sweep rate of 10mVs^{-1}. (d) Corresponding Koutecky–Levich plots (i^{-1} vs. $\omega^{-0.5}$) at different potential from (c) LSV curves. (e) LSV curves of oxygen evolution reaction electrocatalyzed by $NiCo_2S_4$ and Pt/C electrocatalysts in 0.1 M KOH aqueous solution at a sweep rate of 10 mVs^{-1}. (f) Tafel plot of the OER specific activity of $NiCo_2S_4$ and Pt/C.

The electrocatalytic activity can be illustrated by the net peak current density (NPCD), which is calculated by subtracting the background current from the peak current.[6] According to Fig. 5a-b, the NPCD reaches to 0.71 mA cm^{-2} for the $NiCo_2S_4$ SMS, while the commercial Pt/C electrocatalysts exhibit an NPCD of 0.77 mA cm^{-2}. Therefore, the electrocatalytic activity of $NiCo_2S_4$

SMS for ORR approaches that of Pt/C electrocatalyst. To further investigate the ORR kinetics of $NiCo_2S_4$ SMS electrocatalyst, the linear sweep voltammetry (LSV) was carried out on a rotating disk electrode (RDE) at different rotation speeds in O_2-saturated 0.1 M KOH aqueous solution. As shown in Fig. 5c, the LSV curves exhibit similar profiles except the limiting current density increasing with the increasing RDE rotation speed. The corresponding K-L plot of j^{-1} versus $\omega^{-0.5}$ yields straight and parallel lines (Fig. 5d), which implies first-order dependence of O_2 kinetics, as described by Stamenković et al.[28, 29] The number of electron transferred per O_2 molecule was calculated from the K-L plots to be 3.98, which is approximately the theoretical value of 4 throughout the potential range studied (see supplementary information). Thereby, the $NiCo_2S_4$ SMS show excellent electrocatalytic activity for ORR through favorable direct four-electron reaction pathway. The electrocatalytic activity of $NiCo_2S_4$ SMS electrocatalyst for oxygen evolution reaction (OER) was investigated by LSV and Tafel plot, as shown in Fig. 5e-f. In comparison with the Pt/C electrocatalyst, the $NiCo_2S_4$ SMS electrocatalyst exhibits a more negative onset potential for OER with a higher OER current density under the same potential (as shown in Fig. 5e), which indicates that $NiCo_2S_4$ SMS electrocatalyst possesses excellent electrocatalytic activity for OER. The Tafel plot (Fig. 5f) also demonstrates the measured intrinsic electrocatalytical activity of $NiCo_2S_4$ is higher than that of Pt/C electrocatalyst for OER. Moreover, the summary of ORR and OER activities in 0.1 M KOH for $NiCo_2S_4$ and other non-noble electrocatalyst is presented in the supplementary information, which was characterized by LSV on RDE at 1600rpm. It can be seen from Table S1 and Table S2 that the bifunctional catalytic performance of $NiCo_2S_4$ SMS is outstanding in the non-precious metal electrocatalysts. It was also demonstrated that $NiCo_2S_4$ SMS electrocatalyst possess the advantages of methanol tolerance compared with the strong methanol response in the case of Pt/C electrocatalyst[30] (see supplementary information, Fig. S5). In order to better gain insight into the electrocatalytic mechanism of $NiCo_2S_4$ SMS electrocatalyst for both ORR and OER, the detailed analysis of the crystal and electronic structure of $NiCo_2S_4$ was discussed in supplementary information. The excellent electrochemical properties of $NiCo_2S_4$ is originated from the unique d-electronic configuration of Co (III) at the surface of $NiCo_2S_4$, for which the single electron in the e_g energy level selectively occupies the e_g-z^2 orbit pointing to the surface sulfur vacancy and interacting with the frontier orbital of oxygen.

Conclusions

In summary, urchin-like $NiCo_2S_4$ SMS were prepared via a facile synthetic approach. These $NiCo_2S_4$ SMS possess uniform urchin-like morphologies with an average diameter of 0.25 μm and the surface of $NiCo_2S_4$ SMS is decorated by many nano-papillae particles. These urchin-like $NiCo_2S_4$ SMS as non-precious metal electrocatalyst exhibit comparable electrocatalytic activity for ORR and excellent electrocatalytic activity for OER compared with commercial Pt/C electrocatalyst in alkaline solutions. The excellent electrocatalytic property of $NiCo_2S_4$ is originated from the unique d-electronic configuration of Co (III) at the surface of $NiCo_2S_4$. These results will be conductive to the future rational design and development of transition metal thiospinels as highly efficient bifunctional non-precious metal electrocatalysts to replace precious metal electrocatalysts applied in advanced energy conversion and storage devices.

Acknowledgement

This work was supported by National Program on Key Basic Research Project of China (No. MOST2011CB935700), National High Technology Research and Development Program of China (863 Program, No.2013AA050905), the Key Research Program of the Chinese Academy of Sciences (Grant No. KGZD-EW-202-2), National Natural Science Foundation of China (Grant No. 21202178, 21275151, 21271180), the Key Technology Research Projects of Qingdao (No. 12-4-1-24-gx), Science and Technology Program on Basic Research Project of Qingdao (No. 13-1-4-174-jch).

Notes and references

[a] *The Qingdao Key Lab of solar energy utilization and energy storage technology, Qingdao Institute of Bioenergy and Bioprocess Technology, Chinese Academy of Sciences, Qingdao, 266101, P. R. China. Fax: 086-0532-80662746; Tel.: 086-0532-80662746; E-mail: cuigl@qibebt.ac.cn*

[b] *College of Chemistry and Chemical Engineering, Qingdao University, Qingdao, 266071, P. R. China.*

[c] *Qingdao University of Science and Technology, Qingdao, 266042, P. R. China.*

[d] *Beijing Laboratory for Electron Microscopy, Institute of Physics, Chinese Academy of Sciences, Beijing, 100190, P. R. China.E-mail:l.gu@iphy.ac.cn*

θ These authors contributed equally.

† Electronic Supplementary Information (ESI) available: [Experimental section, analysis of catalytic mechanism, other electrochemical characterizations]. See DOI: 10.1039/b000000x/

1 S. B.Yang, L. J. Zhi, K. Tang, X. L. Feng, J. Maier, K. Müllen, *Adv Funct Mater*. 2012, **22**, 3634.

2 Y. Y.Liang, Y. G. Li, H. L.Wang, J. Zhou, J. Wang, T. Regier, H. J. Dai, *Nat. Mater*. 2011, **10**, 780.

3 J.Suntivich, H. A. Gasteiger, N. Yabuuchi, H. Nakanishi, J. B.Goodenough, S. H. Yang, *Nat Chem*. 2011, **3**, 546.

4 J. Suntivich, K. J. May, H. A.Gasteiger, J. B. Goodenough, S. H. Yang, *Science* 2011, **334**, 1383.

5 J.Rodríguez-López, M. A. Alpuche-Aviles, A. J Bard, *J. Am. Chem. Soc*. 2008, **130**, 16985.

6 Z. H. Wen, S. Q. Ci, F. Zhang, X. L. Feng, S. M. Cui, S. Mao, S. L. Luo, Z. He, J. H. Chen, *Adv. Mater.* 2012, **24**, 1399.

7 F. S. Baumann, J. Fleig, M. Konuma, U. Starke, H. U. Habermeier, J. Maier, *J Electrochem Soc*. 2005，**152**, A2074.

8 A. J. Bard, *J. Am. Chem. Soc.* 2010, **132**, 7559.

9 J. Sunarso, A. A. J. Torriero, W. Zhou, P. C. Howlett, M. Forsyth, *J. Phys. Chem. C* 2012, **116**, 5827.

10 A. Singh, S. L. Y. Chang, R. K. Hocking, U. Bach, L. Spiccia, *Energy Environ. Sci.* 2013, **6**, 579.

11 J. L.Shui, N .K Karan, M. Balasubramanian, S. Y. Li, D. J. Liu, *J. Am. Chem. Soc.* 2012, **134**, 16654.

12 L. X. Ding, A. L. Wang, G. R. Li, Z. Q. Liu, W. X. Zhao, C. Y. Su, Y. X. Tong, *J. Am. Chem. Soc.* 2012, **134**, 5730.

13 L. Jörissen, *J. Power Sources* 2006, **155**, 23-32.

14 N. M. Marković, P. N. Ross, *J. Electrochem. Soc.* 1994, **141**, 2590.

15 S. Trasatti, *J. Electroanal. Chem.* 1980, **111**, 125.

16 F. Y. Cheng, J. Shen, B. Peng, Y. Pan, Z. Tao, J. Chen, *Nat Chem.* 2011, **3**, 79.

17 M. R. Gao, J. Jiang, S. H. Yu, *Small* 2012, **8**, 13.

18 H. L. Wang, Y. Y. Liang, Y. G. Li, H. J. Dai, *Angew. Chem. Int. Ed.* 2011, **50**, 10969.

19 W. J. Zhou, X. J. Wu, X. H. Cao, X. Huang, C. L. Tan, J. Tian, H. Liu, J. Y. Wang, H. Zhang. *Energ. Environ. Sci.*, 2013, **6**, 2921.

20 J. Rodríguez-López, A. J. Bard, *J. Am. Chem. Soc.* 2010, **132**, 5121.

21 D. A. Slanac, W. G. Hardin, K. P. Johnston, K. J. Stevenson, *J. Am. Chem. Soc.* 2012, **134**, 8912.

22 J. J. Wang, Y. Q. Wang, F. F. Cao, Y. G. Guo, L. J. Wan, *J. Am. Chem. Soc*. 2010, **132**, 12218

23 O. Knop, K. I. G. Reid, Sutarno,Y. Nakagawa, *Can. J. Chem.* 1968, **46**, 3463.

24 C. H. Huang, O. Knop, *Can. J. Chem.* 1971, **49**, 598.

25 W. H. Bragg, *Nature*. 1915, **95**, 561.

26 A. S. Harvey et al., Phys. *Chem. Chem. Phys.* 2009, 11, 3090.

27 D. P. Shoemaker, J. Li, R. Seshadri, *J. Am. Chem. Soc.* 2009, **131**, 11450.

28 V. Stamenković, T. J. Schmidt, P. N. Ross, N. M. Marković, *J. Phys.Chem. B* 2002, **106**, 11970.

29 V. Stamenković, T. J. Schmidt, P. N. Ross, N. M. Marković, *J. Electroanal. Chem.* 2003, **554-555**, 191.

30 C. L . Lin, J. Rodríguez-López,, A. J Bard,., *Anal. Chem.* 2009, **81**, 8868.

Table of Contents:

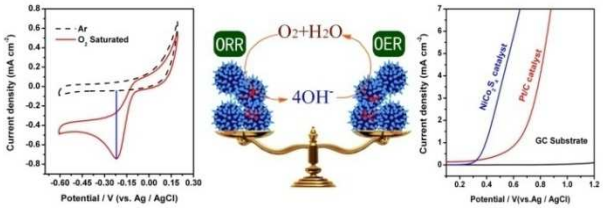

$NiCo_2S_4$ sub-micron spheres with hierarchical architectures pave the way for transition metal thiospinels as efficient bifunctional non-precious metal electrocatalysts